NASA Technical Memorandum 78728

STRESS-INTENSITY FACTORS FOR CORNER CRACKS AT THE EDGE OF A HOLE

I. S. Raju and J. C. Newman, Jr.

JUNE 1978

NASA
National Aeronautics and Space Administration
Langley Research Center
Hampton, Virginia 23665

STRESS-INTENSITY FACTORS FOR CORNER CRACKS AT THE EDGE OF A HOLE

I. S. Raju and J. C. Newman, Jr.
NASA Langley Research Center
Hampton, Virginia

SUMMARY

The literature contains several analytical and experimental evaluations of Mode I stress-intensity factors for corner cracks at holes in plates subjected to remote tension, remote bending, or pin loading in the hole. Unfortunately, these solutions give very different stress-intensity factors for the same crack configuration and loading.

The purpose of this paper is to present stress-intensity factors, calculated by a three-dimensional finite-element analysis, for shallow or deep quarter-elliptical corner cracks at the edge of a hole in a finite-thickness plate. The plate was subjected to remote uniform tension, remote bending, or simulated pin loading in the hole. A wide range of configuration parameters was investigated. The crack depth-to-plate thickness ranged from 0.2 to 0.8, while the ratio of crack depth to crack length ranged from 0.2 to 2. The ratio of hole radius to plate thickness was held at 0.5. To verify the accuracy of the three-dimensional finite-element models employed, convergence was studied by varying the numbers of degrees of freedom (the number ranged from 4400 to 9300). The stress-intensity factor variations along the crack front are compared with solutions from the literature.

INTRODUCTION

Corner cracks at holes are among the most common flaws in aircraft structures. Accurate stress analyses of corner-crack configurations are needed for reliable prediction of crack-growth rates and fracture strengths. However, because of the complexities of such problems, exact solutions are not available. All investigators have used experimental or approximate analytical methods to obtain stress-intensity factors.

Engineering estimates for Mode I stress-intensity factors for some corner-crack configurations have been made by Hall and Finger [1], Liu [2], and Newman [3]. These investigators did not consider the variation of stress-intensity factor along the crack front. Rather, their estimates gave a single value of stress-intensity factor for each crack configuration and, therefore, their estimates might be considered only as an average value of stress-intensity factor along the crack front. Shah [4] used the alternating method, along with an engineering estimate, to calculate the stress-intensity factor variation along the crack front for the corner-crack configuration subjected to either remote tension or pin loading in the hole.

McGowan and Smith [5], Smith, Jolles and Peters [6], and Smith, Peters and Gou [7], used three-dimensional photoelastic techniques to obtain stress-intensity factors for a variety of corner-crack configurations subjected to either remote tension or pin loading in the hole. They reported stress-intensity factors at two or three locations along the crack front.

A few three-dimensional stress analyses of the corner crack configuration have been reported recently. To analyze a quarter-elliptical corner crack emanating from a hole in a finite-thickness plate, Ganong [8] used the alternating method to obtain the stress-intensity-factor variations along the crack front, while Kathiresan [9] and Heckmer and Bloom [10] used three-dimensional finite-element methods. Unfortunately, some of these solutions for the same configuration and loading gave widely varying stress-intensity factors.

The purpose of this paper is to present Mode I stress-intensity factors, calculated by a three-dimensional finite-element analysis [11,12], for shallow or deep quarter-elliptical corner cracks at the edge of a hole in finite-thickness plates. The finite-thickness plates were subjected to remote uniform tension, remote bending, or simulated pin loading in the hole. A wide range of configuration parameters was considered. The ratio of crack depth to plate thickness ranged from 0.2 to 0.8, th ratio of crack depth to crack length ranged from 0.2 to 2, while the ratio of hole radius to plate thickness was held at 0.5. To study convergence, finite-element models with 4400 to 9300 degrees of freedom

were analyzed. The stress-intensity factors were calculated by using a nodal-force method [11]. The stress-intensity-factor variations along the crack front are presented and compared with other solutions from the literature.

SYMBOLS

a	depth of corner crack
b	half-width of cracked plate
c	length of corner crack
F_i	stress-intensity boundary-correction factor
h	half-length of cracked plate
K_I	stress-intensity factor (Mode I)
M	applied bending moment
P	applied load
Q	shape factor for an elliptical crack
R	radius of hole
S_b	remote outer fiber bending stress
S_p	hole bearing stress (= P/2Rt)
S_t	remote uniform tensile stress
t	plate thickness
x,y,z	Cartesian coordinates
θ	angular measurement (see Fig. 5)

σ_n	normal stress applied on hole boundary
ν	Poisson's ratio
ϕ	parametric angle of the ellipse

ANALYSIS

The corner-crack configuration is shown in Figure 1. An elastic plate of thickness t, width 2b and length 2h, contains a through-the-thickness circular hole of radius R. Emanating from the hole are two symmetrically placed quarter-elliptical corner cracks of length c on the front surface and of depth a on the hole surface.

Three types of loading have been considered: remote tension, remote bending, and wedge loading in the hole. The solution for wedge loading in the hole was also used in combination with the remote tension solution to obtain solutions for the case of simulated pin loading in the hole.

Finite-Element Idealization

Two types of elements (isoparametric and singular [13]) were used in combination to model elastic bodies with quarter-elliptical corner cracks. Figure 2 shows a typical finite-element model for a corner crack in a large body, $b/(R+c) \geq 5$ and $h/b = 1.8$. This model idealizes one quarter of the body. Various numbers of wedges were used to form the desired crack configuration in the $y = 0$ plane. A wedge is the region between two radial lines emanating from the point $|x| = R$, $z = 0$ in the $y = 0$ plane, for the circular crack model and is the region between two

hyperbolas in the y = 0 plane for the elliptic crack model as shown in Figure 3. For further details on modelling see Reference 12. The model shown in Figure 2 has eight wedges, each of which is composed of elements around the crack front that are identical in pattern to that shown in the x,y plane. The isoparametric (eight-noded hexahedron) elements were used everywhere except near the crack front. Around the crack front (such as in the x,y plane) each wedge contained eight "singularity" elements in the shape of pentahedrons. The "singularity" elements produced a singular stress field at the crack front. Details of the formulation of these types of elements are given in References 11 and 13 and are not repeated here.

The finite-element model for the quarter-elliptical corner crack was obtained from the finite-element model for the quarter-circular crack by using an elliptic transformation only in the region of the wedges. This transformation was convenient because the nodal forces along the normals to the crack front are used to calculate the stress-intensity factors. If (x,y,z) are the Cartesian coordinates of a node in the circular-crack model and (x',y',z') are the coordinates of that same node in the elliptical-crack model, then the transformation is

$$\left.\begin{aligned} x' = R + (x-R)\sqrt{1 + \frac{c^2-a^2}{(x-R)^2 + z^2}},\ y' = y,\ z' = z \text{ for } \frac{a}{c} \le 1 \\ \text{and} \\ x' = x, y' = y, z' = z\sqrt{1 + \frac{a^2-c^2}{(x-R)^2 + z^2}} \text{ for } \frac{a}{c} > 1 \end{aligned}\right\} \quad (1)$$

for $x \geq R$. Figure 3 shows how circular arcs and radial lines in the x,z plane of the circular-crack model are transformed by equations (1) into ellipses and hyperbolas, respectively, in the x', z' plane of the elliptical-crack model. Because equations (1) are not valid at $x = R$ and $z = 0$, a circle of very small radius, a/1000, was used near $x = R$ and $z = 0$ in the circular crack model. The small circle, which maps onto a very narrow ellipse in the x', z' plane, avoids ill-shaped elements and allows the use of 8-noded elements in the elliptical-crack model. The elliptic transformation reduced the b/c ratio; therefore, to eliminate the influence of plate width, additional rectangular prism elements were added along the x'-axis.

Loading

Three types of loading were applied to the finite-element models of the corner-crack configuration: (1) remote uniform tension, (2) remote bending, and (3) wedge loading in the hole. The loadings are illustrated in Figure 4. The remote uniform tension is S_t in Figure 4a; the remote outer fiber bending stress, S_b, in Figure 4b is calculated from the applied bending moment; and the applied normal stress on the hole boundary, σ_n, in Figure 4c was assumed to be given by

$$\sigma_n = \frac{3P}{4Rt} \sin^2\theta \qquad (2)$$

where P is the total applied force acting in the y-direction over the arc from $\theta = 0$ to π. The particular form of σ_n was chosen to simulate pin loading (see Fig. 5). The mode I stress-intensity factor for the case of pin loading in the hole is obtained by appropriate superposition of the results for remote uniform tension (Fig. 4a) and for wedge loading in the hole (Fig. 4c). (See Ref. 3)

Stress-Intensity Factor

Only loadings which cause Mode I (tension) deformations were analyzed The Mode I stress-intensity factor, K_I, at any point along the quarter-elliptical corner crack in a finite-thickness plate was taken to be

$$K_I = S_i \sqrt{\pi \frac{a}{Q}} F_i \left(\frac{a}{t}, \frac{a}{c}, \frac{R}{t}, \phi\right) \qquad (3)$$

where the subscript i denotes the type of applied loading (remote tension (i=t), remote bending (i=b), or wedge loading in the hole (i=p)); Q is the shape factor for an ellipse and is given by the square of the complete elliptic integral of the second kind [15]. The boundary-correction factor, F_i, is a function of crack depth, crack length, hole radius, plate thickness, and the parametric angle of the ellipse. Note that the length and width of the plate were chosen large enough so that they would have a negligible effect on stress intensity. Values for F_i were

calculated as a function of $\frac{a}{t}$, $\frac{a}{c}$ and ϕ for $\frac{R}{t} = 0.5$. The $\frac{a}{c}$ ratios ranged from 0.2 to 2 and the $\frac{a}{t}$ ratios ranged from 0.2 to 0.8.

The stress-intensity factor (Mode I) for the simulated pin-loaded configuration shown in Figure 5 was obtained by superposition of the results for the configurations shown in Figures 4a and 4c. (Superposition of these results gives the correct normal stresses for the pin-load configuration only along the $y = 0$ plane.) For this case, the Mode I stress-intensity factor is given by

$$K_I = S_p \sqrt{\pi \frac{a}{Q}} \frac{1}{2} \left(\frac{R}{b} F_t + F_p\right) \tag{4}$$

where $S_p = P/2Rt$, and F_t and F_p are the boundary-correction factors obtained from equation 3 for remote tension and wedge loading in the hole, respectively. (This superposition method gives no information on Mode II stress-intensity factors.)

The stress-intensity factors from the finite-element models of the quarter-elliptical corner cracks were obtained by using a nodal-force method, details of which are given in Reference 11. In this method, the nodal forces normal to the crack plane and ahead of the crack front are used to evaluate the stress-intensity factor. In contrast, the crack-opening displacement (COD) method presented in [13] requires a prior assumption of either plane stress or plane strain, which is a potential source of inaccuracy. The nodal-force method requires no such assumption.

RESULTS AND DISCUSSION

In the following sections, results for quarter-circular and quarter-elliptical corner cracks emanating from a circular hole (R/t = 0.5) subjected to various loading are presented. Convergence of the stress-intensity factors for a deep quarter-elliptical corner crack was studied by varying the number of degrees of freedom in the finite-element models from 4400 to 9300. The stress-intensity factor variations along the crack front for quarter-circular (a/c = 1) and quarter-elliptical (a/c = 0.2 and 2) corner cracks are presented as functions of a/t with R/t = 0.5. The stress-intensity factors are compared with other solutions and experimental results from the literature.

Convergence

In reference 11, the present method was applied to the problems of embedded circular (a/c = 1) and embedded elliptical (a/c = 0.2) cracks in a large body under uniform tension. Because the results obtained for these crack shapes were generally within 1 percent of the exact solutions [15], the present method is expected to be suitable for analyses of the more complex configurations considered herein, provided that enough degrees of freedom are used to ensure convergence.

Figure 6 shows the results of the convergence study for a deep quarter-elliptical corner crack (a/c = 0.2, a/t = 0.8, R/t = 0.5). This

configuration was chosen because proximity of the back surface to the crack front was expected to cause convergence difficulties. Four finite-element models with 4400 to 9300 degrees of freedom (DOF) were analyzed. These models used 2, 4, 8 or 10 wedges to idealize the elliptic crack front on the $y = 0$ plane. A typical eight-wedge model is shown in Figure 2. The two-, four-, and eight-wedge models had equal wedge angles. The ten-wedge model had nonuniform wedges with smaller wedges near the intersection of the crack with the hole surface ($\phi = \pi/2$). The smaller wedges near the free surface were used to study the "boundary-layer" effect suggested by Hartranft and Sih [16]. The idealization used to model the circular hole was the same for all models (see Fig. 2). The two finest models (8454 and 9306 degrees of freedom) gave stress-intensity factors within less than one percent of each other except at the intersection of the crack front and the hole surface, where the difference was about 5 percent. The ten-wedge model with about 9300 degrees of freedom was used subsequently to obtain stress-intensity factors for all other crack configurations.

Quarter-Circular Corner Cracks

Figure 7 shows the normalized stress-intensity factors for a quarter-circular corner crack as a function of the parametric angle, ϕ, and the crack-depth-to-plate-thickness ratio, a/t, for remote tension, remote

bending, or wedge loading in the hole. For all loading types considered, the smaller a/t ratios generally gave higher normalized stress-intensity factors. For remote tension and for wedge loading in the hole, the maximum normalized stress-intensity factor occurs near the intersection of the crack with the hole surface ($\phi = \pi/2$). For remote bending, the normalized stress-intensity factor was largest at $\phi = 0$ (front surface). The negative stress-intensity factors shown in Figure 7b for a/t = 0.8 are, of course, meaningful only in the presence of sufficient tensile loading to prevent contact between the crack surfaces.

The stress-intensity factors (Mode I) for quarter-circular corner cracks subjected to simulated pin loading, as shown in Figure 5, can be obtained from the results shown in Figures 7a and 7c by use of equation 4.

Figures 8a and 8b show stress-intensity factors obtained by several investigators for a quarter-circular corner crack in a finite-thickness plate under remote tension. Figure 8a shows the results for a corner crack with a/t = 0.2 and R/t = 0.5. The present results are shown as solid circular symbols. Shah's estimate [4] is about 6 percent higher than the present results. The results from Heckmer and Bloom [10] are 10 to 20 percent higher than the present results near the free surfaces ($\phi = 0$ and $\pi/2$), but only about 3 percent higher in the interior. The photoelastic results [5,7], which represent the experimental stress-intensity value at the approximate midpoint of each photoelastic slice, generally agree well with the present results.

The stress intensity is less near the intersection of the crack with the hole surface ($\phi = \pi/2$) than just below the surface. This behavior agrees qualitatively with that proposed by Hartranft and Sih [16]. Note that the wedge angles near $\phi = \pi/2$ are smaller than those near $\phi = 0$. Similar refinements in the wedge angles near $\phi = 0$ would probably have revealed lower stress-intensity factors in that region as well.

Figure 8b shows the results for a deeper corner crack ($a/t = 0.5$) than that shown in Figure 8a. Shah's estimate [4] is within 10 percent of the present results, except that Shah does not predict the lower stress intensity near $\phi = \pi/2$. Kathiresan's results [9] are 10 to 20 percent lower than the present results. This descrepancy may be attributed to the fact that the present study employed over three and one-half times as many degrees of freedom as did Kathiresan's. Ganong's results [8], which are for a single corner crack emanating from a hole, are 25 percent higher than the present results. The results for a single corner crack are expected to be lower than those for two corner cracks [4]. Again, the photoelastic results from Smith, Peters, and Gou [7] agreed to within ±10 percent with the present results.

Some of the discrepancies between the various finite-element solutions may be attributed to the method used to extract the stress-intensity factor from the three-dimensional analyses. Figure 9 shows the stress-intensity factor variation along the crack front for a typical corner-crack configuration as determined from the present analysis by two methods. The configuration and loading are those appropriate to Figure 8a. The stress-intensity factors were determined from the crack-opening displacements (COD)

assuming either plane stress or plane strain and from the nodal forces ahead of the crack front [11]. The stress-intensity factors calculated from the COD method assuming plane strain were about 10 percent higher than those obtained assuming plane stress. Results from the nodal-force method fell generally between the two COD results. Because neither plane-strain nor plane-stress conditions are fully realized in a corner-cracked plate, either assumption is expected to lead to some inaccuracy in stress-intensity factors.

Quarter-Elliptical Corner Cracks

Figures 10 and 11 show the normalized stress-intensity factors for quarter-elliptical corner cracks (a/c = 0.2 and 2, respectively) as a function of the parametric angle, ϕ, and the crack-depth-to-plate-thickness ratio, a/t, for remote tension, remote bending, or wedge loading in the hole.

Figure 10 (a/c = 0.2) shows that for remote tension, the larger a/t ratios gave higher normalized stress-intensity factors, but for remote bending or wedge loading the trend was generally reversed. For remote bending, the maximum normalized stress-intensity factor occurred near $\phi = \pi/2$ for a/t = 0.2 and at $\phi = 0$ for a/t = 0.8. The wedge-loaded hole results (Fig. 10c) showed a steep gradient in stress-intensity factor near the hole surface.

Figure 11 (a/c = 2) shows that for remote tension and bending the smaller a/t ratios gave higher normalized stress-intensity factors. For

remote tension and wedge loading, the stress-intensity factors varied little (about 10 to 15 percent) along the crack front compared to those for the other crack configurations (a/c = 0.2 and 1). For remote bending, the normalized stress-intensity factor was largest at $\phi = 0$ (front surface). Again, the negative stress-intensity factors shown in Figure 11b for a/t = 0.8 are meaningful only in the presence of sufficient tensile loading to prevent crack-surface contact.

The stress-intensity factors (Mode I) for quarter-elliptical corner cracks subjected to simulated pin loading, as shown in Figure 5, can be calculated by substituting into equation 4 the results shown in Figures 10a and 10c for a/c = 0.2, and Figures 11a and 11c for a/c = 2. Figure 12 shows the normalized stress-intensity factors for quarter-elliptical corner cracks (a/c = 0.2, 1.0, and 2.0) as a function of the parametric angle, ϕ, and the crack-depth-to-plate-thickness ratio, a/t, for simulated pin loading. The graphs are similar to those shown for the wedge-loaded case, differing mainly in magnitude. This similarity is due to the small R/b ratios considered here, which caused the contributions from the remote tension case to be small compared with those from the wedge-loaded case. As in the wedge-loaded case, for quarter-elliptic corner cracks with a/c = 0.2 the stress-intensity factors rise sharply with increasing ϕ near the intersection of the crack with the hole surface. For quarter-circular corner cracks, the maximum stress-intensity factor occurs near $\phi = \pi/2$. For quarter-elliptic cracks with a/c = 2, the stress-intensity factors are relatively constant along the crack front.

CONCLUDING REMARKS

A three-dimensional finite-element elastic stress analysis was used to calculate Mode I stress-intensity factor variations along the crack front for two symmetrical quarter-elliptical corner cracks at the edge of a hole in a finite-thickness plate. The plates were subjected to remote uniform tension, remote bending, wedge loading in the hole or simulated pin loading in the hole. The ratio of crack depth to plate thickness ranged from 0.2 to 0.8, and the ratio of crack depth to crack length ranged from 0.2 to 2, while the ratio of hole radius to plate thickness was held at 0.5. Three-dimensional singularity elements in the shape of pentahedrons were used at the crack front; elsewhere, eight-noded hexahedrons were used. A nodal-force method which requires no prior assumption of either plane stress or plane strain was used to evaluate the stress-intensity factors.

A convergence study on stress-intensity factors for a deep quarter-elliptical corner crack in a finite-thickness plate showed satisfactory convergence. About 9300 degrees of freedom were used in calculating stress-intensity factors for all corner-crack configurations.

For quarter-circular corner cracks subjected to tension or wedge loading in the hole, the maximum stress-intensity factor occurred near the intersection of the crack with the hole surface, whereas for bending it occurred at the intersection of the crack with the front surface.

For quarter-elliptical corner cracks (crack-depth-to-crack-length ratio of 0.2) subjected to tension or wedge loading in the hole, the

maximum stress-intensity factor occurred near the intersection of the crack with the hole surface for shallow cracks (crack-depth-to-plate-thickness less than or equal to 0.5) but occurred at the front surface for deep cracks (crack-depth-to-plate-thickness ratio of 0.8).

The stress-intensity factors for quarter-elliptical corner cracks (crack depth-to-crack length ratio of 2) were nearly constant (within about 10 percent) along the crack front in the cases of tension and wedge loading in the hole, though not in the case of bending, where the stress intensity factor was greatest at the intersection of the crack with the front surface.

For quarter-elliptical corner cracks subjected to simulated pin loading in the hole (balanced by uniform tension at one end), the stress-intensity variations along the crack front were similar to those obtained for wedge loading in the hole, differing mainly in magnitude.

The stress-intensity factors obtained herein should be useful in correlating fatigue-crack-growth rates and in calculating fracture toughness for the corner-crack configurations considered.

REFERENCES

[1] Hall, L. R. and Finger, R. W.: Fracture and Fatigue Growth of Partially Embedded Flaws, AFFDL-TR-70-144, U.S. Air Force, Dec. 1970.

[2] Liu, A. F.: Stress Intensity Factor for a Corner Flaw, Engr. Fracture Mechanics, Vol. 4, 1972, pp. 175-179.

[3] Newman, J. C., Jr.: Predicting Failure of Specimens With Either Surface Cracks or Corner Cracks at Holes, NASA TND-8244, June 1976.

[4] Shah, R. C.: Stress Intensity Factors for Through and Part-Through Cracks Originating at Fastener Holes, ASTM STP-590, 1976, pp. 429-459.

[5] McGowan, J. J.; and Smith, C. W.: Stress Intensity Factors for Deep Cracks Emanating From the Corner Formed by a Hole Intersecting a Plate Surface, ASTM STP-590, 1976, pp. 460-476.

[6] Smith, C. W.; Jolles, M. I.; and Peters, W. H.: Stress Intensity for Cracks Emanating From Pin Loaded Holes, VPI-E-76-13, Virginia Polytech. Inst. & State Univ., Aug. 1976.

[7] Smith, C. W.; Peters, W. H.; and Gou, S. F.: Influence of Flaw Geometries on Hole-Crack Stress Intensity, to be presented at the Eleventh National Symposium on Fracture Mechanics, Blacksburg, VA, June 1978.

[8] Ganong, G. P.: Quarter-Elliptical Cracks Emanating From Holes in Plates, Ph.D. Thesis, Colorado State University, Fort Collins, Colorado, July 1975.

[9] Kathiresan, K.: Three-Dimensional Linear Elastic Fracture Mechanics Analysis by a Displacement Hybrid Finite Element, Ph.D. Thesis, Georgia Institute of Technology, Atlanta, Georgia, Sept. 1976.

[10] Hechmer, J. L.; and Bloom, J. M.: Determination of Stress Intensity Factors for the Corner-Cracked Hole Using the Isoparametric Singularity Element, International Journal of Fracture, Oct. 1977.

[11] Raju, I. S.; and Newman, J. C., Jr.: Three-Dimensional Finite-Element Analysis of Finite-Thickness Fracture Specimens, NASA TND-8414, May 1977.

[12] Raju, I. S.; and Newman, J. C., Jr.: Improved Stress-Intensity Factors for Semi-Elliptical Surface Cracks in Finite-Thickness Plates, NASA TMX-72825, Aug. 1977. (To be published in International Journal of Fracture).

[13] Tracey, D. M.: "Finite Element for Three-Dimensional Elastic Crack Analysis," Nucl. Engr. and Design, Vol. 26, 1974.

[14] Barsoum, R. S.: "On the Use of Isoparametric Finite Elements in Linear Fracture Mechanics," Int. J. Num. Meth. Engr., Vol. 10, no. 1, January 1976.

[15] Green, A. E.; and Sneddon, I. N.: The Distribution of Stress in the Neighborhood of a Flat Elliptical Crack in an Elastic Solid, Proc. Cambridge Phil. Soc., 46, 1959.

[16] Hartranft, R. J.; and Sih, G. C.: An Approximate Three-Dimensional Theory of Plates With Application to Crack Problems, Int. J. Eng. Sci., Vol 8, No. 8, Aug 1970.

TABLE I: Stress-Intensity Boundary-Correction Factors, F_i, for Quarter-Elliptical Corner Cracks Subjected to Remote Tension, Remote Bending, and Wedge Loading in the Hole

($F_i = K_I/S_i\sqrt{\pi a/Q}$; $b/(R+c) \geq 5$; $h/b = 1.8$; $\nu = 0.3$)

TYPE OF LOADING	a/c	0.2			1			2		
	$\frac{2\phi}{\pi}$ \ $\frac{a}{t}$	0.2	0.5	0.8	0.2	0.5	0.8	0.2	0.5	0.8
TENSION	0	0.673	0.878	1.256	1.832	1.699	1.808	1.603	1.353	1.259
	0.125	0.711	0.934	1.255	1.870	1.699	1.763	1.607	1.350	1.235
	0.25	0.833	1.061	1.385	1.886	1.675	1.673	1.588	1.322	1.187
	0.375	0.989	1.215	1.547	1.936	1.687	1.608	1.566	1.297	1.144
	0.5	1.141	1.360	1.707	2.015	1.733	1.608	1.532	1.272	1.109
	0.625	1.298	1.500	1.832	2.119	1.817	1.640	1.486	1.252	1.088
	0.75	1.477	1.643	1.930	2.247	1.951	1.750	1.446	1.253	1.095
	0.833	1.682	1.796	2.020	2.359	2.107	1.907	1.406	1.263	1.123
	0.917	1.949	2.018	2.148	2.447	2.267	2.122	1.375	1.295	1.184
	0.958	2.128	2.257	2.366	2.398	2.347	2.274	1.296	1.276	1.198
	1.0	1.885	2.276	2.554	1.985	2.072	2.164	1.053	1.088	1.054
BENDING	0	0.635	0.713	0.729	1.562	1.279	1.113	1.291	0.977	0.824
	0.125	0.649	0.699	0.661	1.520	1.172	0.969	1.226	0.871	0.672
	0.25	0.729	0.722	0.632	1.432	1.005	0.722	1.121	0.710	0.453
	0.375	0.832	0.759	0.605	1.371	0.864	0.497	1.025	0.563	0.253
	0.5	0.922	0.779	0.556	1.332	0.744	0.293	0.935	0.436	0.081
	0.625	1.005	0.785	0.489	1.311	0.647	0.118	0.852	0.333	-0.059
	0.75	1.090	0.791	0.411	1.310	0.580	-0.028	0.787	0.263	-0.162
	0.833	1.177	0.806	0.351	1.315	0.548	-0.130	0.739	0.226	-0.221
	0.917	1.276	0.830	0.302	1.311	0.536	-0.205	0.704	0.209	-0.260
	0.958	1.310	0.846	0.262	1.247	0.518	-0.239	0.651	0.197	-0.267
	1.0	1.084	0.770	0.219	0.984	0.417	-0.246	0.515	0.160	-0.236
WEDGE LOADED	0	0.071	0.071	0.086	0.638	0.462	0.419	0.471	0.531	0.412
	0.125	0.076	0.065	0.083	0.669	0.480	0.420	0.465	0.522	0.415
	0.25	0.096	0.075	0.092	0.698	0.498	0.413	0.449	0.499	0.413
	0.375	0.129	0.093	0.105	0.743	0.530	0.417	0.433	0.476	0.413
	0.5	0.176	0.122	0.126	0.803	0.581	0.446	0.426	0.459	0.419
	0.625	0.251	0.167	0.156	0.879	0.657	0.501	0.398	0.447	0.434
	0.75	0.369	0.242	0.204	0.966	0.762	0.594	0.384	0.447	0.462
	0.833	0.516	0.353	0.278	1.041	0.872	0.707	0.371	0.453	0.495
	0.917	0.714	0.533	0.408	1.101	0.972	0.848	0.364	0.470	0.541
	0.958	0.854	0.722	0.587	1.091	1.019	0.947	0.342	0.467	0.558
	1.0	0.797	0.818	0.759	0.917	0.978	0.927	0.277	0.401	0.497

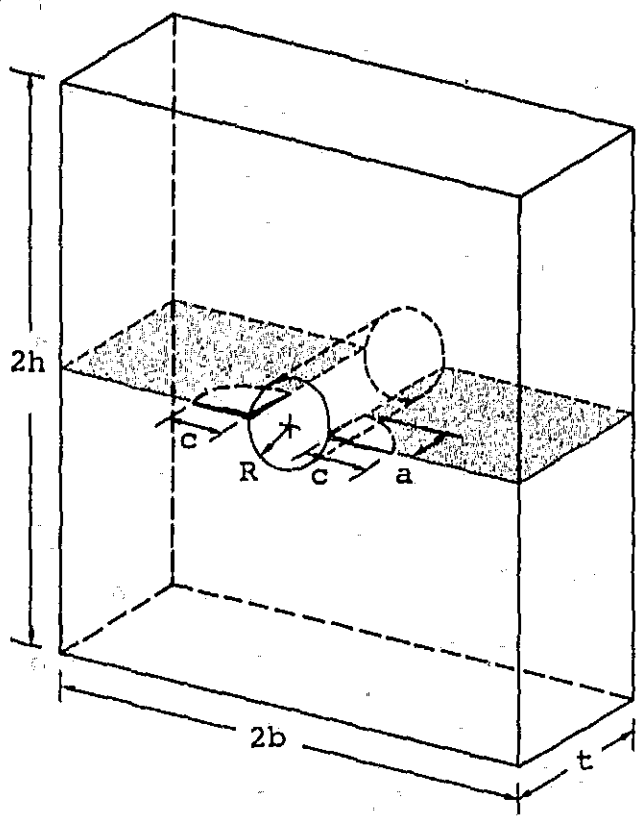

Fig. 1.- Corner cracks at the edge of a hole in a finite plate.

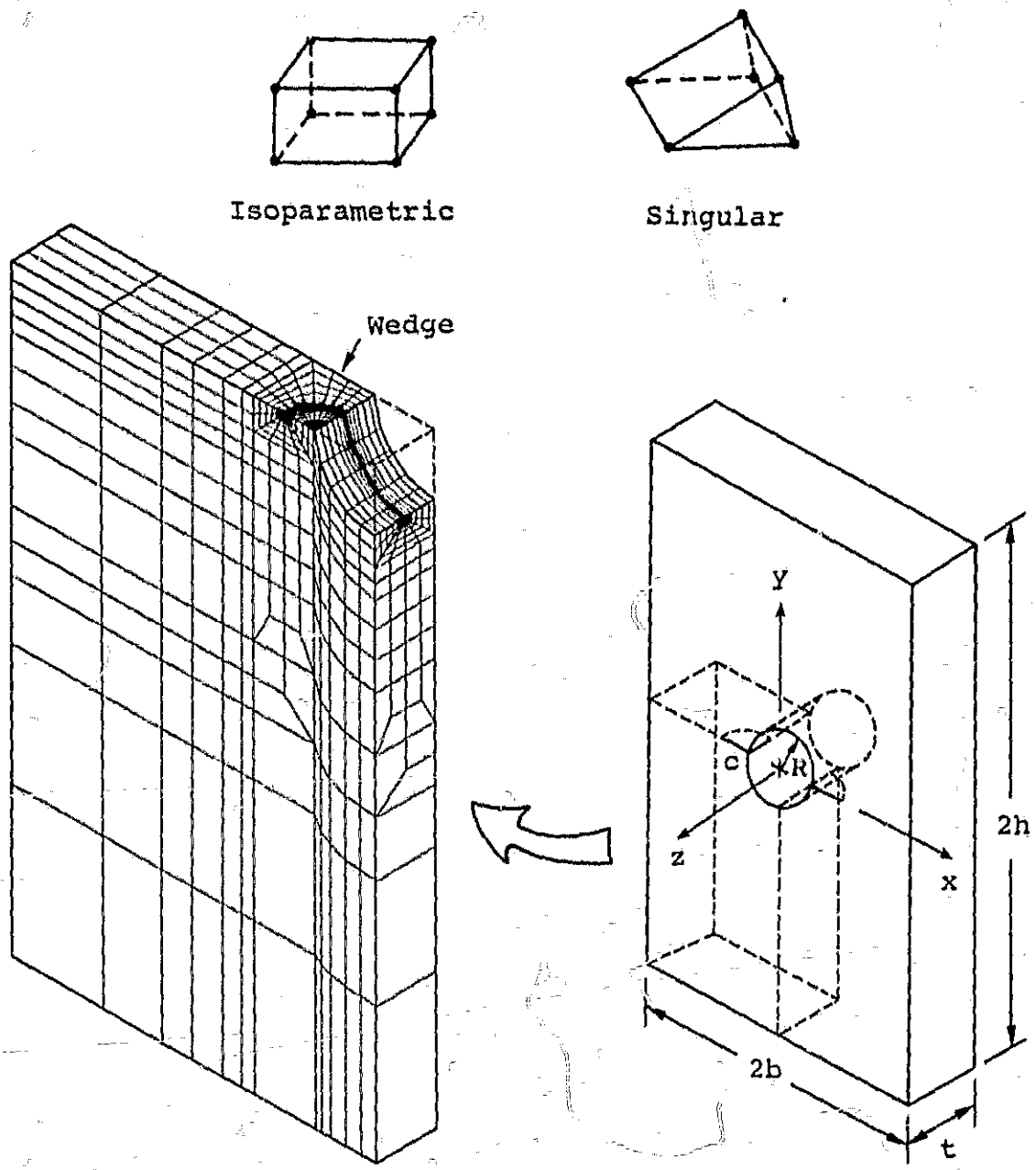

Fig. 2.- Finite-element idealization of the corner-crack configuration.

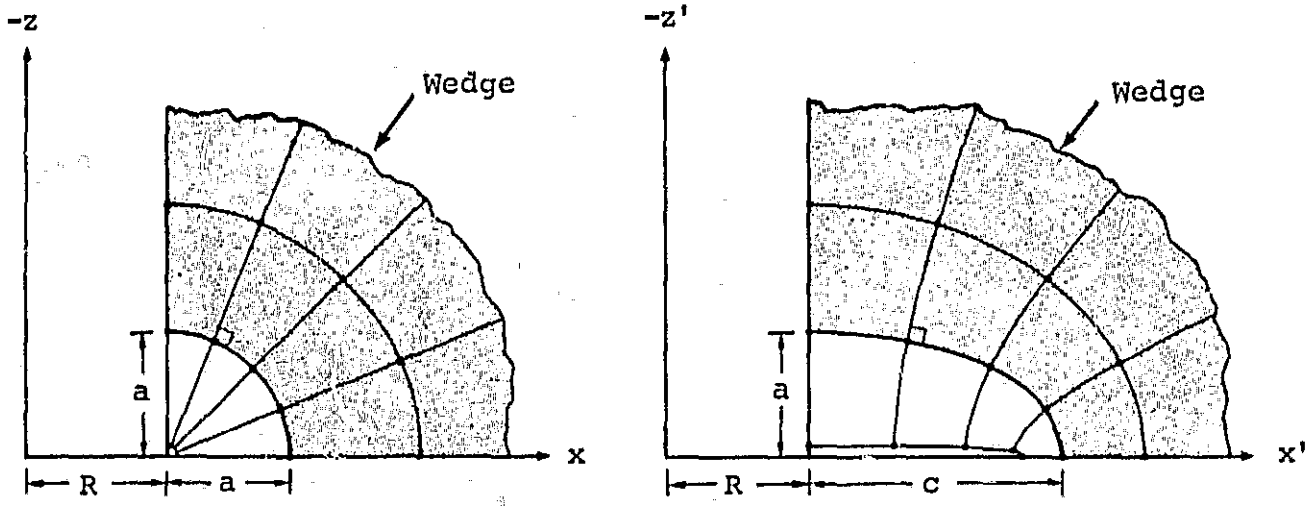

(a) Quarter-circular crack

(b) Quarter-elliptic crack

Fig. 3.- Circle to ellipse transformation (y = y' = 0).

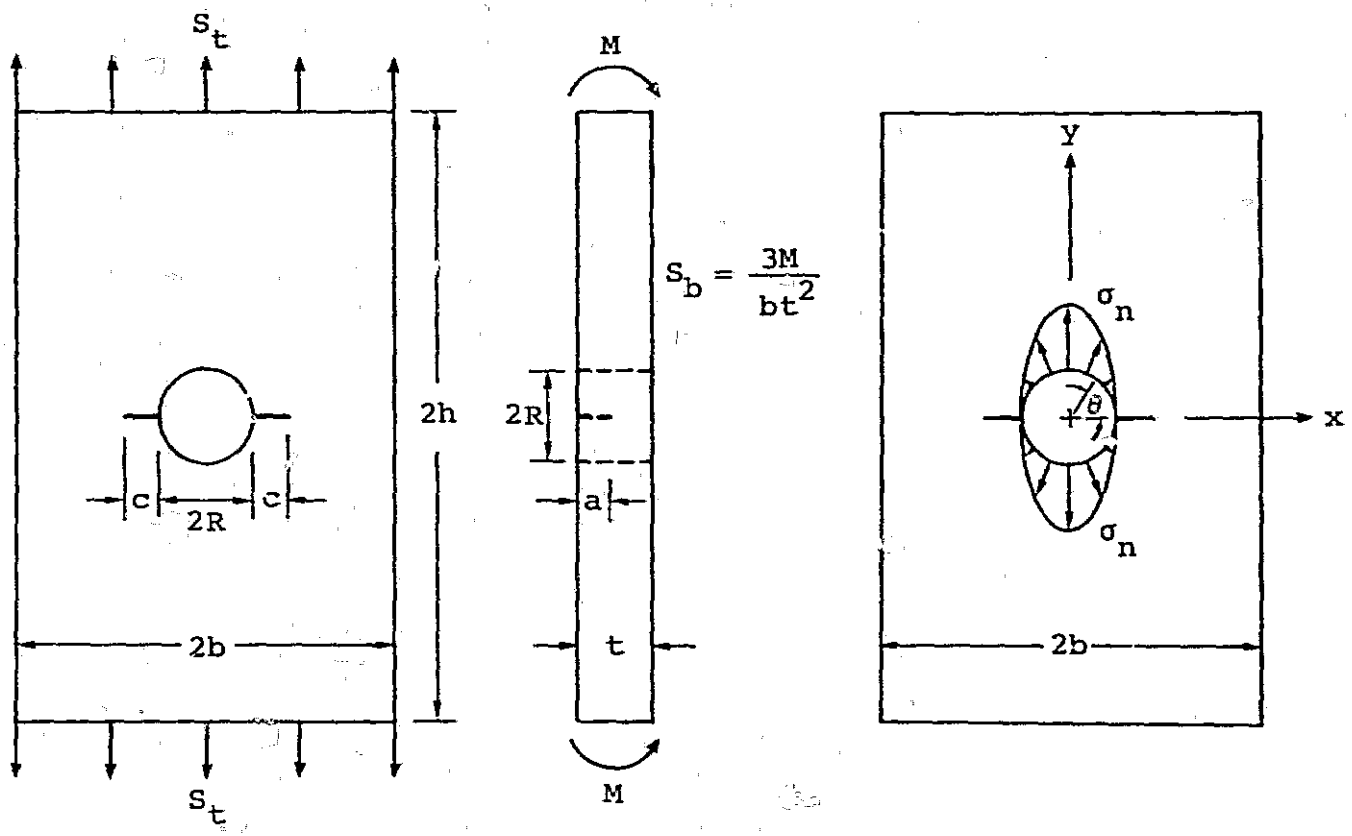

(a) Tension (b) Bending (c) Wedge loaded hole

Fig. 4.- Corner-crack configuration subjected to various loads.

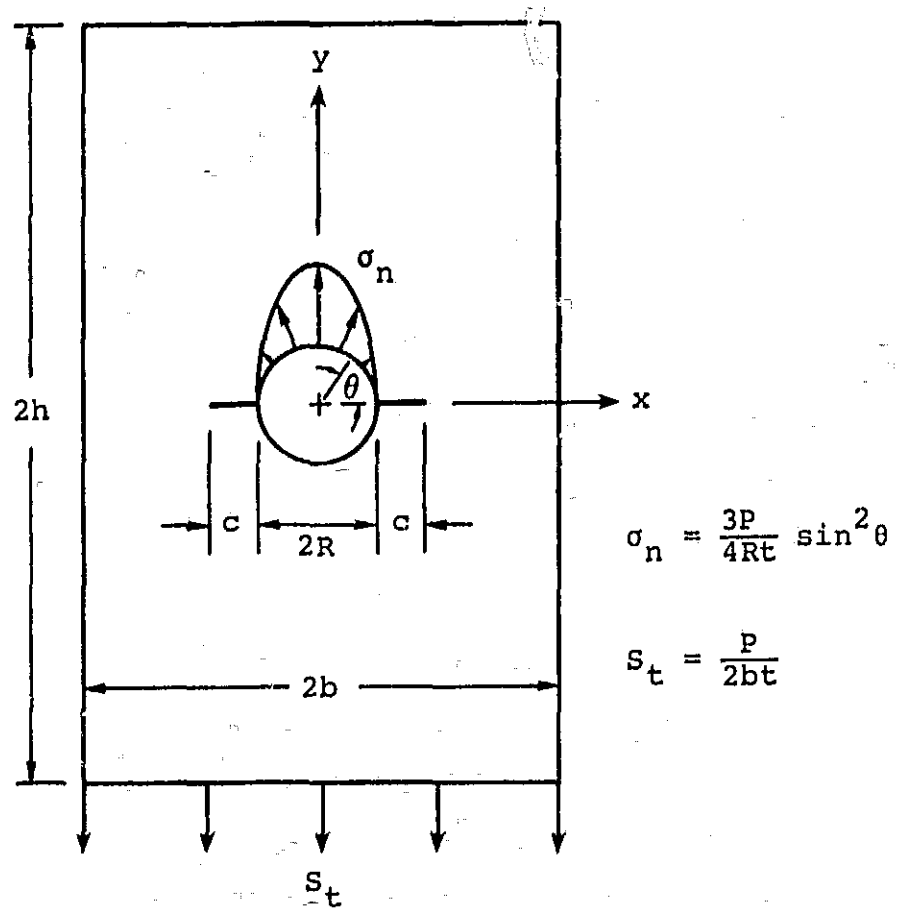

Fig. 5.- Corner-crack configuration subjected to simulated pin loading.

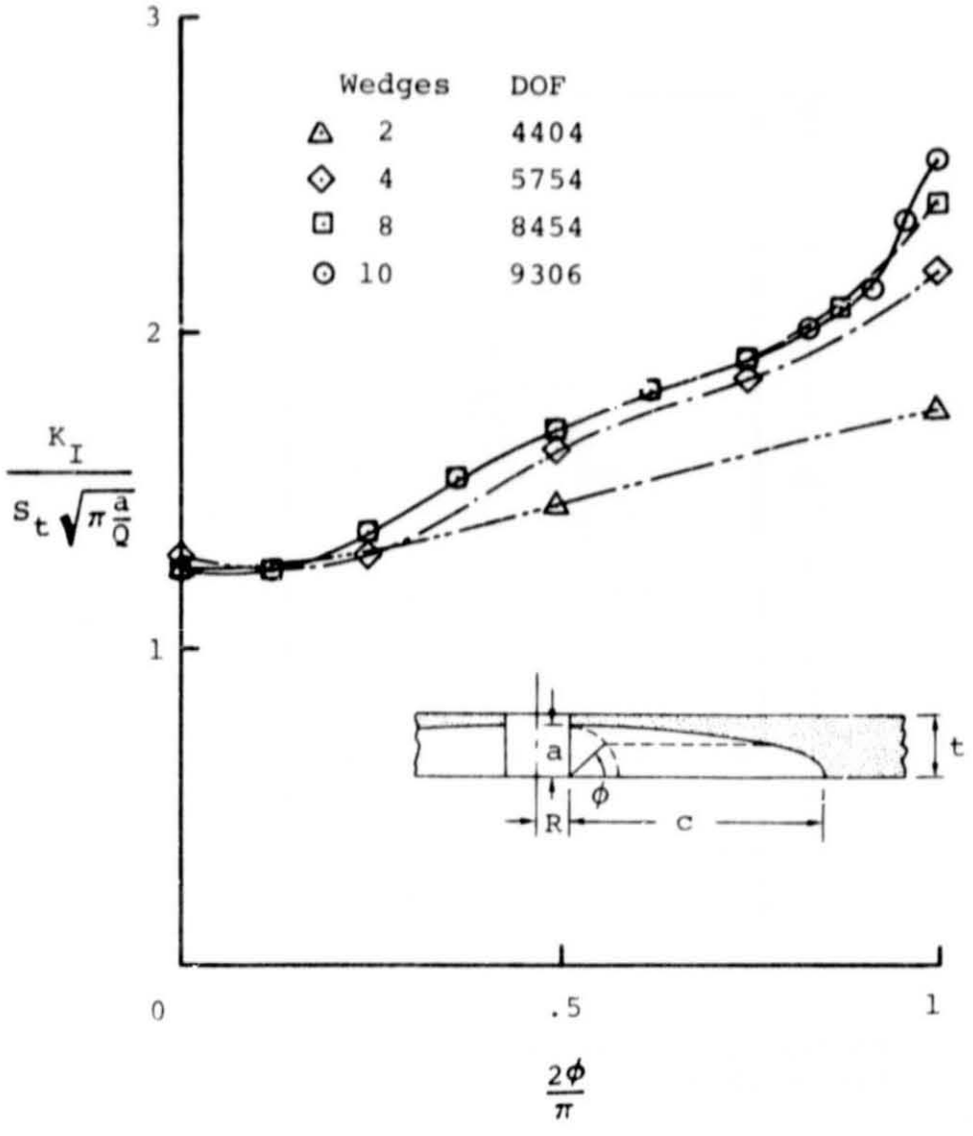

Fig. 6.- Convergence of stress-intensity factors for a deep quarter-elliptic corner cracks (a/t = 0.8; a/c = 0.2; R/t = 0.5).

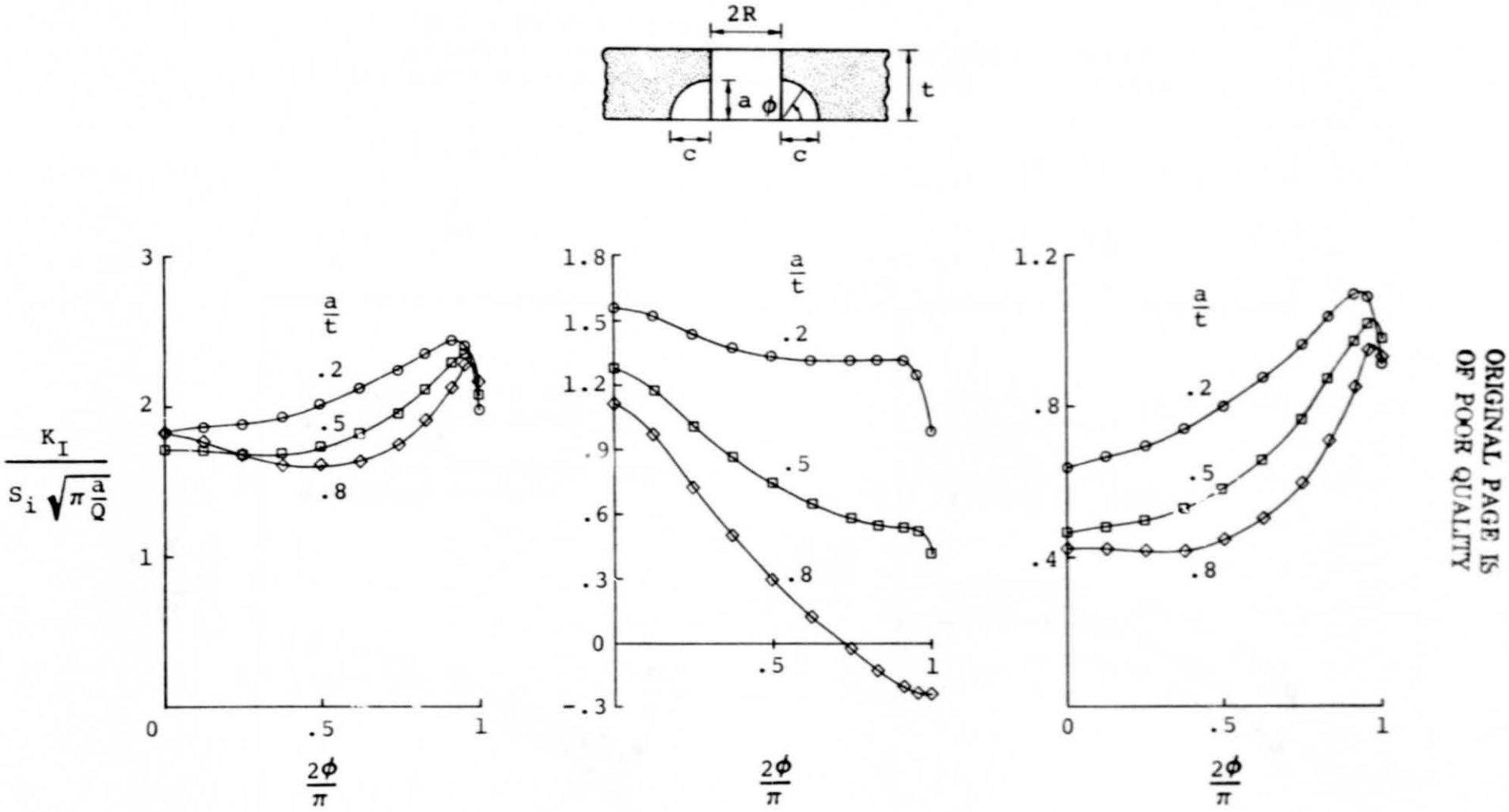

Fig. 7.- Distribution of stress-intensity factors along crack front for quarter-circular corner cracks (a/c = 1; R/t = 0.5).

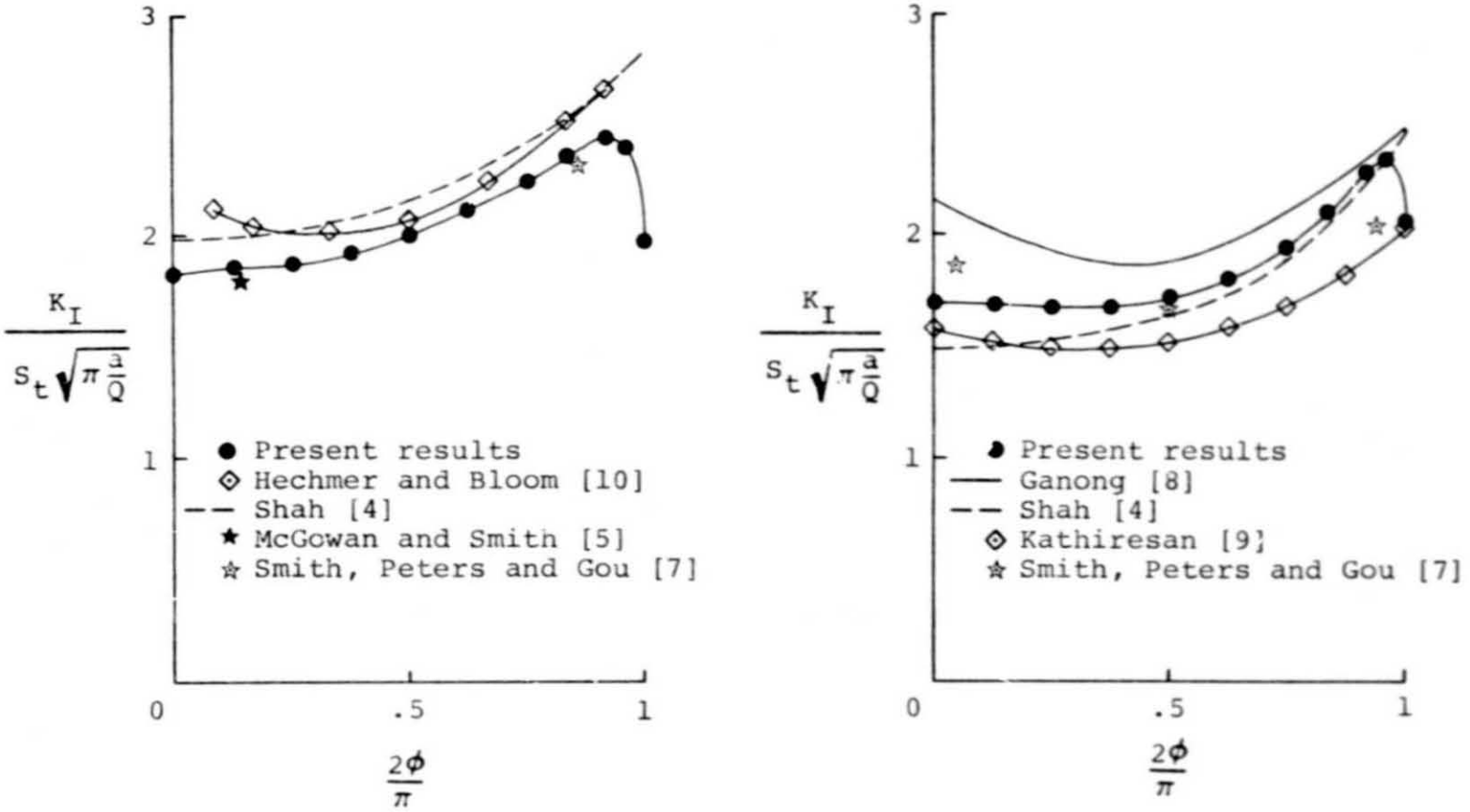

(a) a/t = 0.2

(b) a/t = 0.5

Fig. 8.- Comparison of stress-intensity factors for quarter-circular corner cracks subjected to remote tension (a/c = 1; R/t = 0.5).

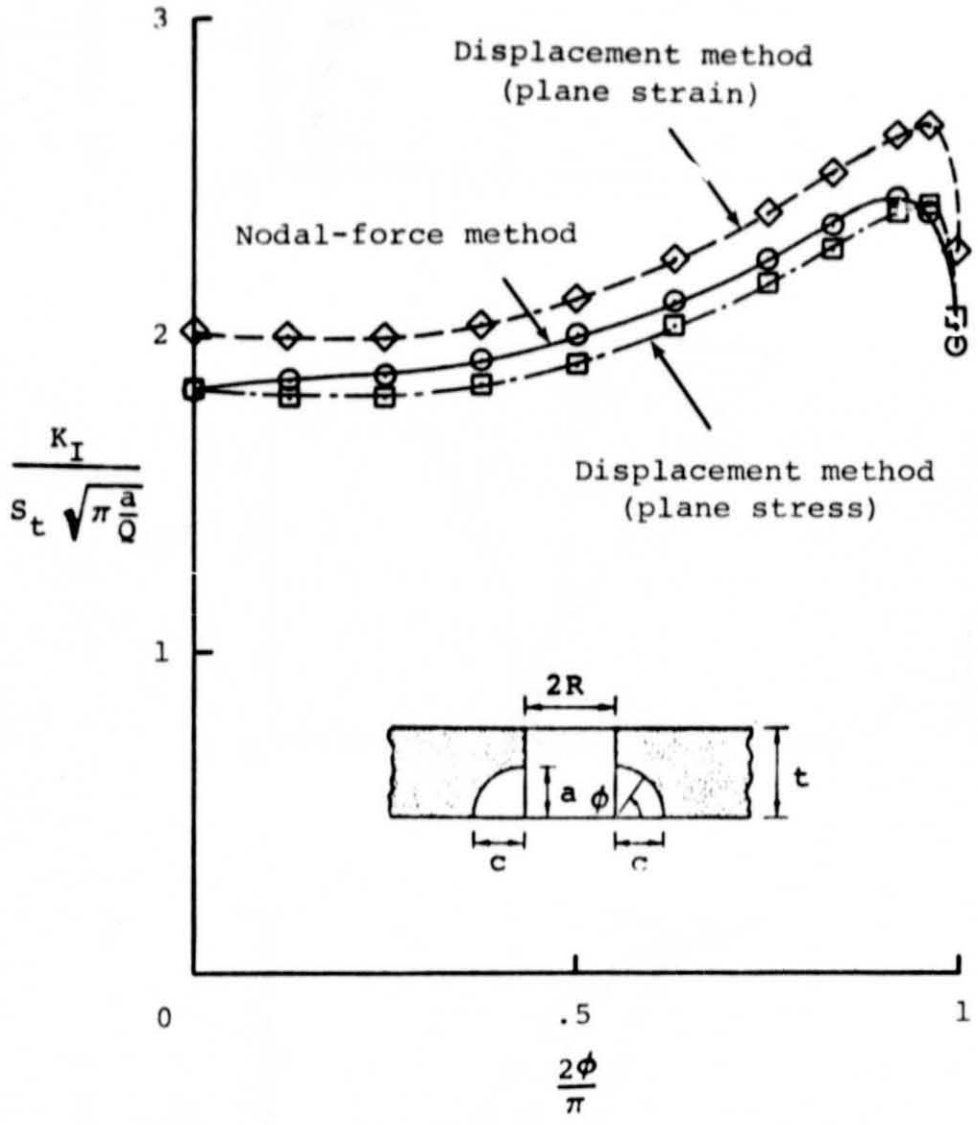

Fig. 9.- Comparison of stress-intensity factors determined by displacement method (plane stress and plane strain) and nodal-force method (a/c = 1; a/t = 0.2; R/t = 0.5).

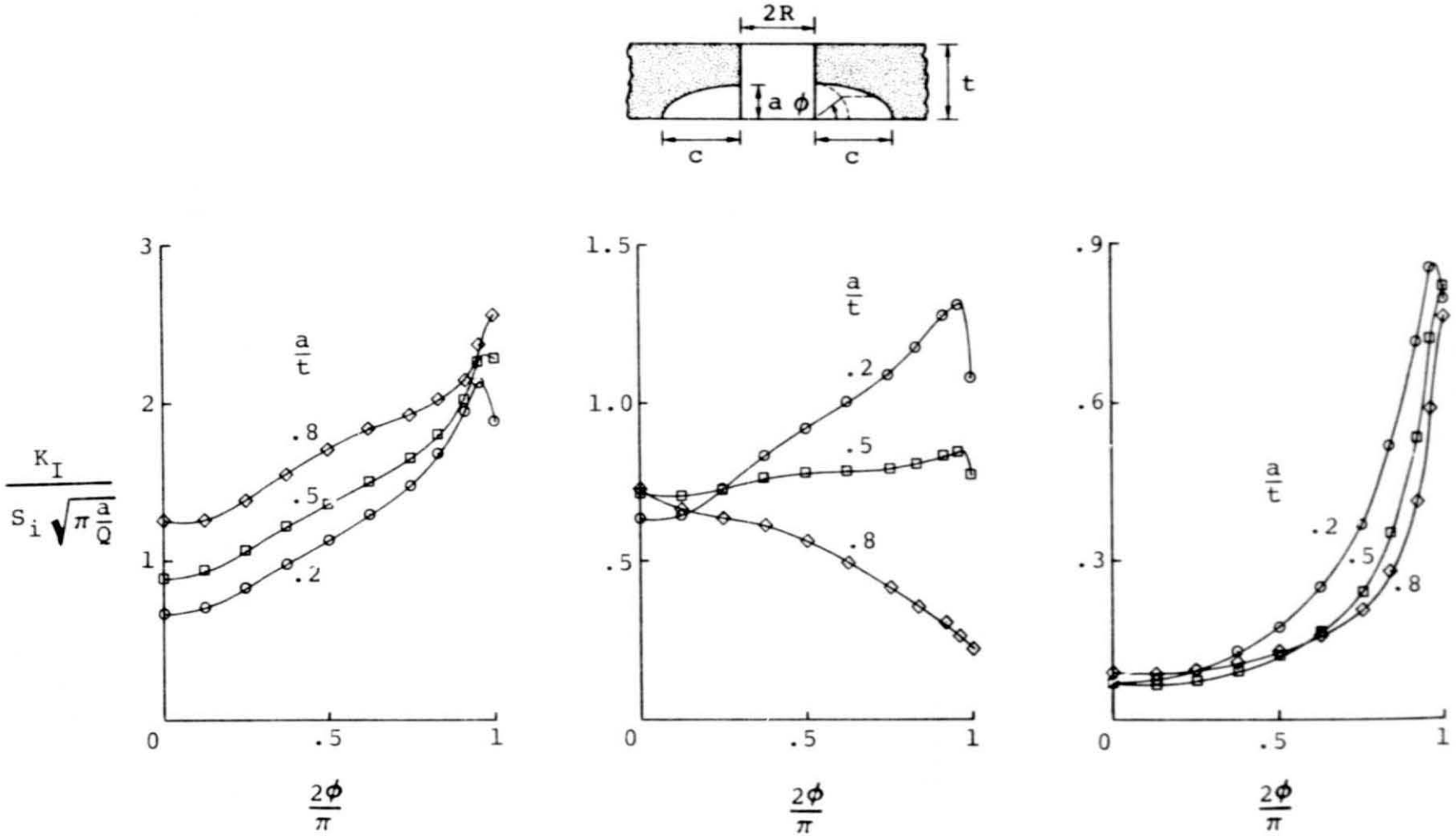

Fig. 10.- Distribution of stress-intensity factors along crack front for quarter-elliptic corner cracks (a/c = 0.2; R/t = 0.5).

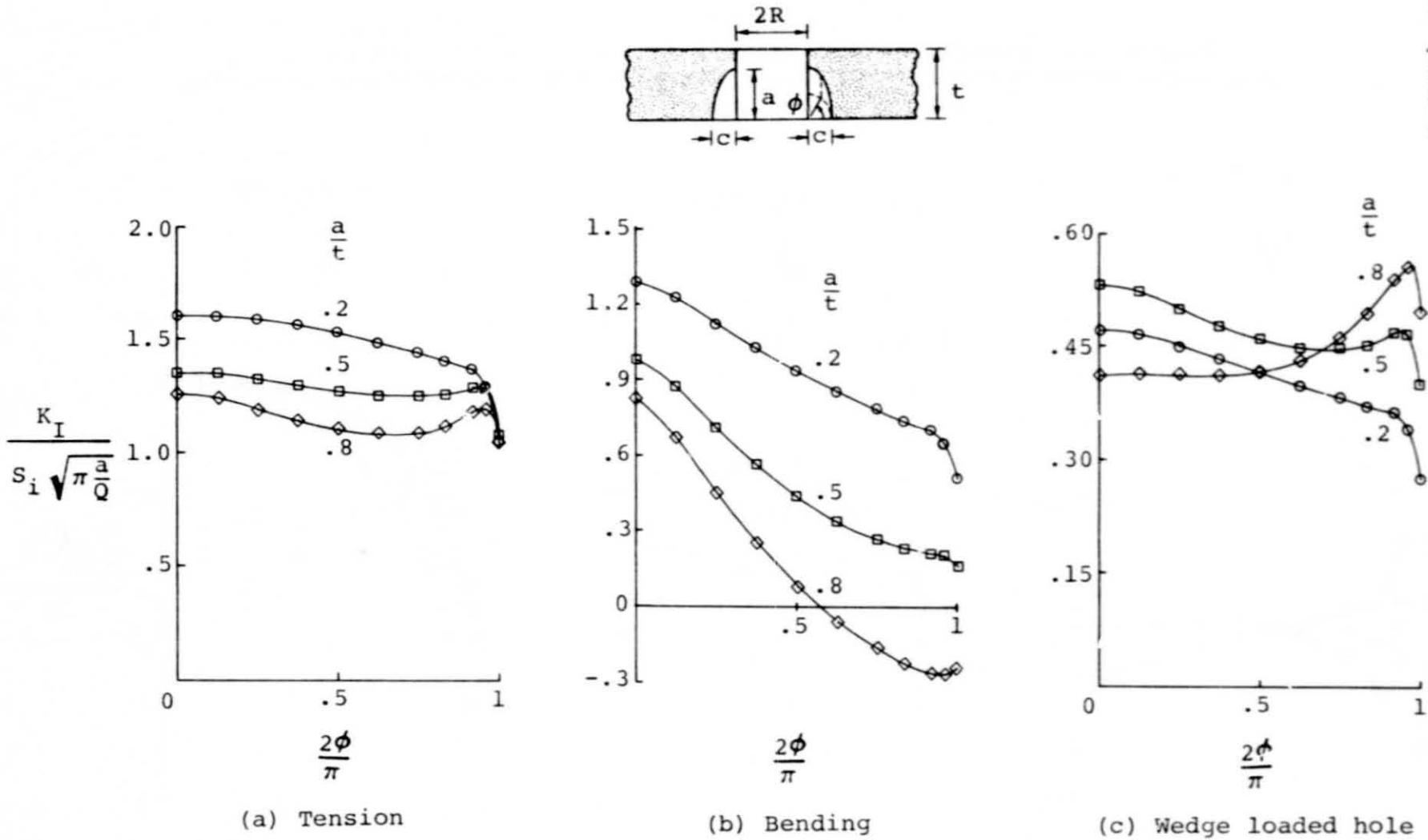

Fig. 11 - Distribution of stress-intensity factors along crack front for quarter-elliptic corner cracks (a/c = 2; R/t = 0.5).

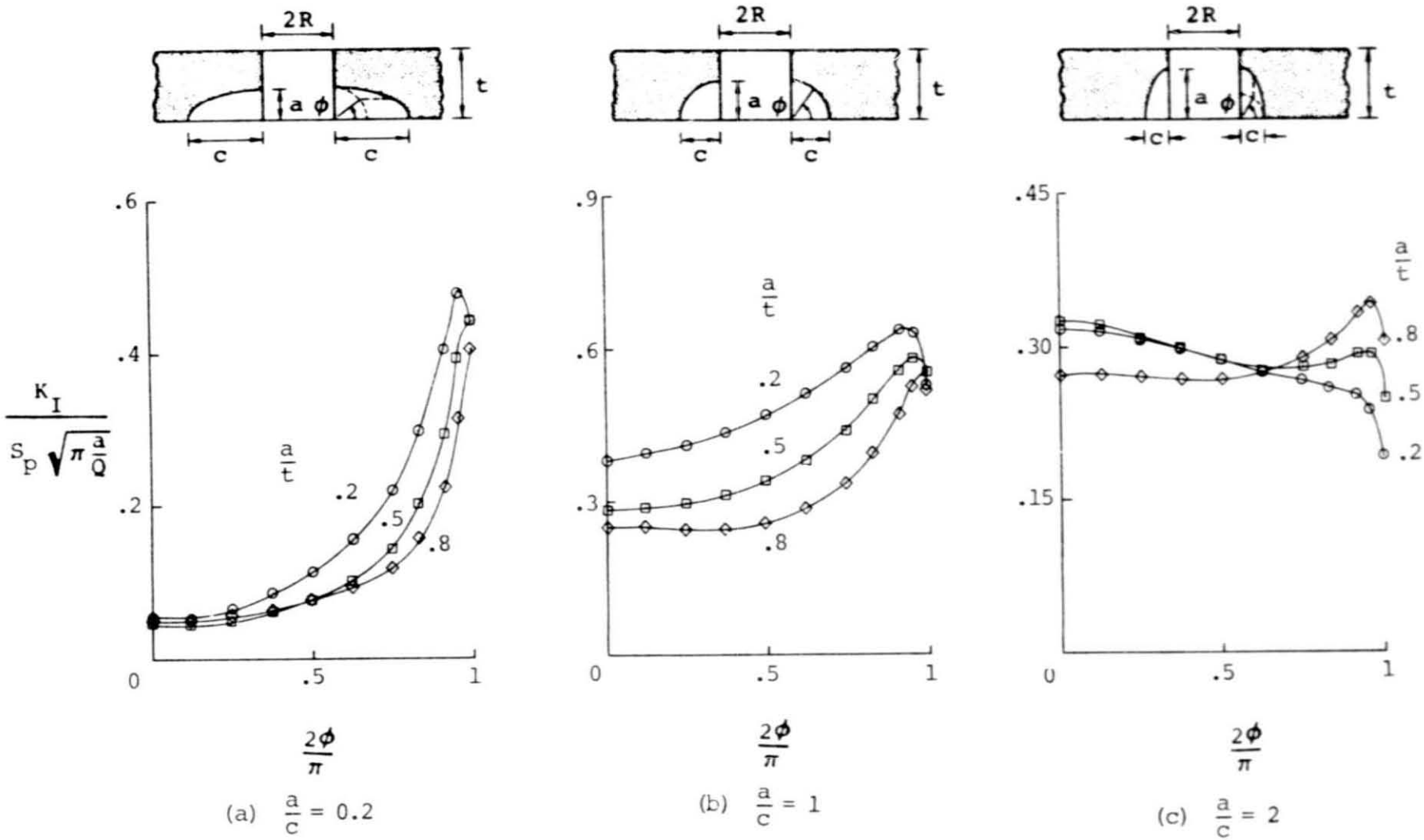

Fig. 12.- Distribution of stress-intensity factors along crack front for quarter-elliptic corner cracks under simulated pin loading (R/t = 0.5).